

# Design of the Subaru laser guide star adaptive optics module

Makoto Watanabe<sup>a</sup>, Hideki Takami<sup>a</sup>, Naruhisa Takato<sup>a</sup>, Stephen Colley<sup>a</sup>, Michael Eldred<sup>a</sup>, Thomas Kane<sup>a</sup>, Olivier Guyon<sup>a</sup>, Masayuki Hattori<sup>a</sup>, Miwa Goto<sup>a</sup>, Masanori Iye<sup>b</sup>, Yutaka Hayano<sup>a,b</sup>, Yukiko Kamata<sup>b</sup>, Nobuo Arimoto<sup>b</sup>, Naoto Kobayashi<sup>c</sup>, and Yosuke Minowa<sup>c</sup>

<sup>a</sup>Subaru Telescope, National Astronomical Observatory of Japan,  
650 North A'ohoku Place, Hilo, Hawaii 96720, USA;

<sup>b</sup>National Astronomical Observatory of Japan, 2-21-1, Osawa, Mitaka, Tokyo 181-8588, Japan;

<sup>c</sup>Institute of Astronomy, University of Tokyo, 2-21-1, Osawa, Mitaka, Tokyo 181-0015, Japan

## ABSTRACT

The laser guide star adaptive optics (AO) module for the Subaru Telescope will be installed at the  $f/13.9$  IR Nasmyth focus, and provides the compensated image for the science instrument without change of the focal ratio. The optical components are mounted on an optical bench, and the flexure depending on the telescope pointing is eliminated. The transferred field of view for the science instrument is 2 arcmin diameter, but a 2.7 arcmin diameter field is available for tip-tilt sensing. The science path of the AO module contains five mirrors, including a pair of off-axis parabolic mirrors and a deformable mirror. It has also three additional mirrors for an image rotator. The AO module has a visible 188-element curvature based wavefront sensor (WFS) with photon-counting avalanche photodiode (APD) modules. It measures high-order terms of wavefront using either of a single laser (LGS) or natural guide star (NGS) within a 2 arcmin diameter field. The AO module has also a visible  $2 \times 2$  sub-aperture Shack-Hartmann WFS with 16 APD modules. It measures tip-tilt and slow defocus terms of wavefront by using a single NGS within a 2.7 arcmin diameter field when a LGS is used for high-order wavefront sensing. The module has also an infrared  $2 \times 2$  sub-aperture Shack-Hartmann WFS with a HgCdTe array as an option. Both high- and low-order visible WFSs have their own guide star acquisition units with two steering fold mirrors. The AO module has also a source simulator. It simulates LGS and NGS beams, simultaneously, with and without atmospheric turbulence by two turbulent layer at about 0 and 6 km altitudes, and reproduces the isoplanatism and the cone effect for the LGS beam.

**Keywords:** adaptive optics, laser guide star, wavefront sensing, curvature sensor, Subaru telescope

## 1. INTRODUCTION

The Subaru laser guide star adaptive optics (AO) module will be located on the IR Nasmyth platform of the Subaru Telescope. It includes the optics, sensors, and electronics needed to compensate the input  $f/13.9$  science beam and relay it to a science instrument at the same focal ratio. All optical and opto-mechanical components of this module are mounted on one optical bench, and the sensors and electronics (except computers) are stored in the racks below and nearby the optical bench. Figure 1 shows the optical layout on the optical bench. The optics consists of three major parts: 1) Science path, 2) three wavefront sensors (WFSs) including a visible high-order WFS and two low-order WFSs operating in the visible and near-infrared region, and 3) a calibration unit. Table 1 summarizes the major specifications of the AO module.

In the initial conceptual design,<sup>1</sup> the location of the AO module was planned to be at the Cassegrain focus, and similar optical and mechanical designs to those of the current NGS36 system<sup>2,3</sup> were incorporated. However, the beam size on the deformable mirror (DM) was limited to 61 mm in diameter because of the limitation of size of the optics owing to the limited mechanical space at the Cassegrain. This limitation on the DM was a large drawback to achieve an enough DM stroke for the new higher order system.

The change in location to the Nasmyth allows us to increase the beam size on the DM by employing the larger optics. It also provides several other advantages: 1) increasing an additional mechanical space for WFSs,

---

Further author information: (Send correspondence to M. W.)

M. W.: E-mail: watanabe@naoj.org

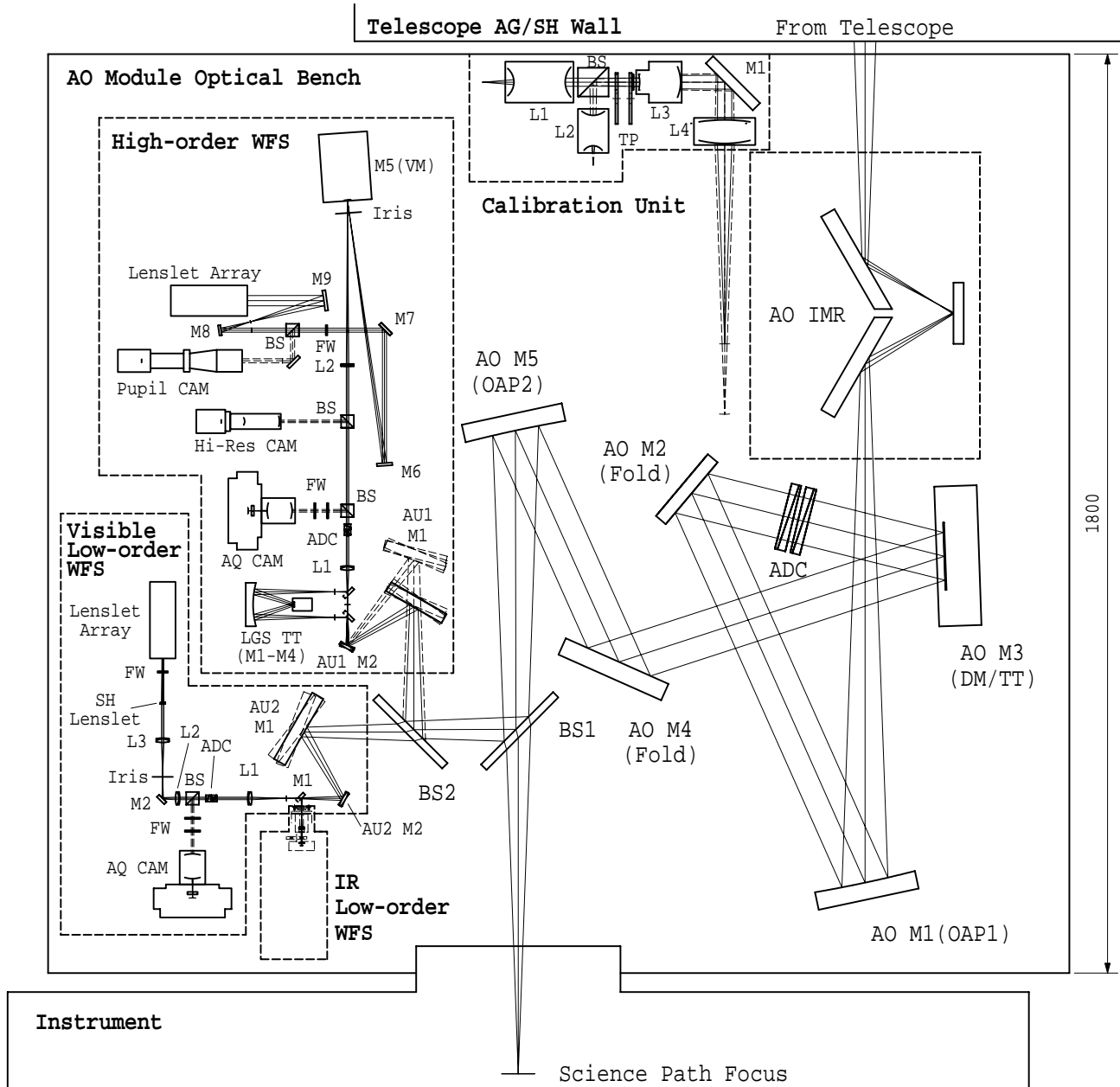


Figure 1. Optical layout of AO module.

calibration unit, and electronics, 2) increasing the flexibility for the optical and mechanical design, 3) eliminating the flexure depending on the telescope pointing, 4) increasing the accessibility to the system, and 5) allowing to test the system independently of the telescope operation. On the other hand, it has disadvantages of decreasing the throughput and increasing the emissivity due to the additional mirrors of the telescopes ternary and the image rotator.

In this proceeding, the optical design of the AO module is mainly presented. The project summary, the performance simulation, the detail of the DM, and the laser system are presented in other papers.<sup>4-7</sup>

**Table 1.** Major specifications of AO Module.

Science Path	
Spectral coverage	0.45–5 $\mu\text{m}$ for transmission
Input & output focal ratio	$f/13.9$
FOV (for science instrument)	2 arcmin (in diameter)
FOV (for WFSs)	2.7 arcmin (in diameter)
DM type	Bimorph mirror with 188 electrodes
Beam diameter on DM	90 mm
Actuator type of TTM for DM	Voice coils
Tip-tilt stroke of TTM for DM	$\pm 5$ arcsec (@ sky)
Number of beam splitters (BS1)	4
High-order WFS	
Sensor type	188-element curvature sensor
Target guide star	LGS / NGS
Spectral coverage	0.45–1.0 $\mu\text{m}$
Detectors	Photon counting APD modules
FOV	4 arcsec (in diameter)
Patrolled FOV	2 arcmin (in diameter)
Visible low-order WFS	
Sensor type	$2 \times 2$ sub-aperture Shack-Hartmann sensor
Target guide star	NGS
Spectral coverage	0.45–1.0 $\mu\text{m}$
Detectors	Photon counting APD modules
FOV	3.5 arcsec (in diameter)
Patrolled FOV (in diameter)	3 arcmin
Infrared low-order WFS (option)	
Sensor type	$2 \times 2$ sub-aperture Shack-Hartmann sensor
Target guide star	NGS
Spectral coverage	0.9–2.5 $\mu\text{m}$
Detector	$128 \times 128$ pixel HgCdTe array
FOV	4 arcsec (in diameter)
Patrolled FOV	2.7 arcmin (in diameter)
Calibration unit	
Number of light source	LGS: 1, NGS: 1
Spectral coverage	LGS: 0.589 $\mu\text{m}$ , NGS: 0.589–2.2 $\mu\text{m}$
Simulated FOV	LGS: 0.2 arcmin, NGS: 2 arcmin (in diameter)
Number of turbulent plates	2
Simulated altitudes of turbulent layers	$\sim 0, 6$ km
Opto-mechanics	
Overall dimension of optical bench	2000(W) $\times$ 1800(L) $\times$ 250(H) mm

## 2. SCIENCE PATH

### 2.1. Optical Layout

The science path includes 1) a K-type image rotator (IMR) to compensate for the field rotation at the Nasmyth focus, 2) a pair of off-axis parabolic (OAP1 & OAP2) mirrors to collimate and refocus the input beam, 3) a bimorph-type deformable mirror (DM) on a fast tip-tilt mount (TTM), 4) an atmospheric dispersion corrector (ADC) to compensate for the atmospheric dispersion, 5) two fold mirrors (AO M2 & M4), and 6) an exchangeable beam splitter (BS1) to split the light between the science instrument and the WFSs.

The two OAP mirrors are identical ( $f = 1201$  mm, off-axis angle 24 degrees, 200 mm diameter). The OAP1 collimates the  $f/13.9$  input beam into the collimated beam with a 90 mm diameter, forming an image of the telescope pupil (the telescope's secondary mirror) on the DM. The OAP2 re-images the beam, keeping the same focal length and exit pupil distance as the originals (110.6 m and 17.6 m, respectively).

The tip-tilt control will be done at the DM. Therefore, the DM will be mounted in a TTM rather than having a separate tip-tilt mirror. The range of the tilt angle is  $\pm 5$  arcsec on the sky. This TTM will be built by Observatoire de Paris, Meudon in France, and it has a similar design to that of the ESO MACAO system.<sup>8,9</sup>

In the collimated beams, an ADC is insertable. It has a conventional design, which consists of two identical doublet prisms of S-BAH27 and S-LAH60 glasses. This ADC corrects the atmospheric dispersion in both visible and infrared wavelength over 0.45–2.2  $\mu\text{m}$  for both science instrument and WFSs. When the zenith angle is small so that the correction is not needed for the science instrument, this ADC is removed and other ADCs in the WFSs are used for the correction in the visible wavelength instead.

The transferred field of view (FOV) for the science instrument is 2 arcmin in diameter. However, the transferred FOV for the WFSs is quite larger (2.7 arcmin in diameter) in order to extend the sky coverage of the natural guide star (NGS) for the low-order wavefront (tip-tilt and defocus) sensing when the laser guide star (LGS) is used for the higher-order correction.

The BS1 is placed at a distance of 670 mm before the focus of the OAP2, and is tilted by 45 degrees to reflect visible light (shortward of around 1  $\mu\text{m}$ ) into the WFS paths. We are planning to install four BS1 at once on the optical bench to select the desirable range of wavelengths for wavefront sensing. The BS1 is made from  $\text{CaF}_2$ , the size is 200 mm  $\times$  145 mm, and the thickness is 15 mm. It has a slight wedge to avoid an astigmatism introduced by BS1.

## 2.2. Throughput and Emissivity

Table 2 shows the throughput and emissivity estimates for the science path including the telescope. For Al and Ag mirrors, the reflectivities are based on the measurements for the telescope or for the current NGS36 system with a protected silver coating. For others, they are taken from the typical catalog values.

**Table 2.** Throughput and emissivity estimates for the science path.

Wavelength ( $\mu\text{m}$ )	Throughput					Emissivity
	0.60	0.90	1.25	1.65	2.20	2.20
Telescope (1 Al + 2 Ag mirrors)	0.849	0.830	0.927	0.939	0.931	0.069
IMR (3 Ag mirrors)	0.921	0.896	0.946	0.955	0.958	0.042
AO (5 Ag mirrors)	0.872	0.833	0.912	0.926	0.931	0.069
BS1 (1 BS + 1 glass surfaces)	0.941	0.941	0.941	0.941	0.941	0.060
<b>Overall without ADC</b>	<b>0.642</b>	<b>0.582</b>	<b>0.752</b>	<b>0.781</b>	<b>0.781</b>	<b>0.219</b>
ADC (4 glass surfaces)	0.961	0.961	0.961	0.961	0.961	0.039
<b>Overall with ADC</b>	<b>0.616</b>	<b>0.559</b>	<b>0.722</b>	<b>0.750</b>	<b>0.750</b>	<b>0.250</b>

## 2.3. Image Quality

Figure 2 shows the imaging performance of the science path. Unfortunately, at the Infrared Nasmyth focus, a small coma aberration is introduced by the telescope. This reason is that the Nasmyth focus has a slight deviation from the Ritchey-Chretien system because the secondary mirror is common to the Infrared Cassegrain focus and its figure is optimized for Cassegrain, not Nasmyth. However, it is still acceptable within the science field (2 arcmin in diameter), which is nearly diffraction limited.

# 3. WAVEFRONT SENSORS

## 3.1. High-order WFS

### 3.1.1. Optical layout

The high-order WFS is a visible 188-element curvature based wavefront sensor with photon counting APD modules, and measures high-order terms of wavefront using either of a single LGS or NGS. It includes 1) a guide star acquisition unit (AU1 M1 & M2) to acquire a guide star from a 2 arcmin diameter field, 2) a fast

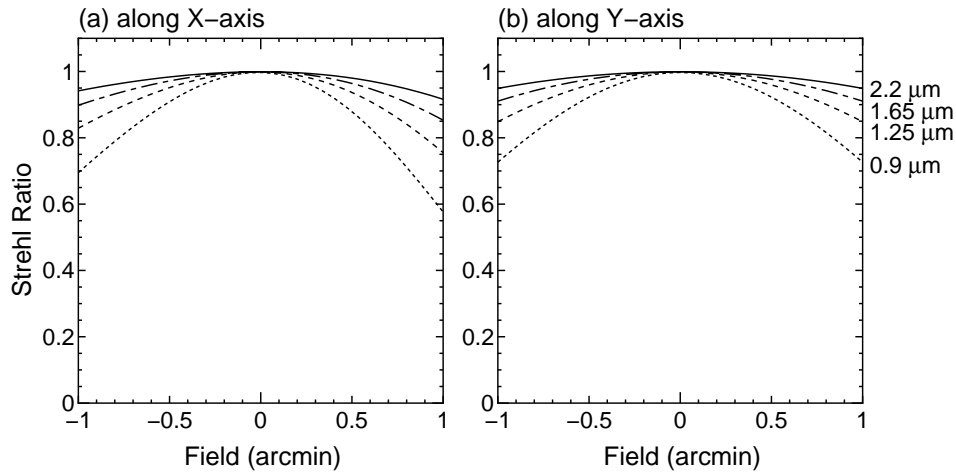


**Figure 2.** Strehl ratio representing monochromatic imaging performance of science path at 0.9, 1.25, 1.65, and 2.2  $\mu\text{m}$ . The figure (a) and (b) show the performance along the parallel and perpendicular axes to the optical bench, respectively.

tip/tilt mirror with an Offner relay (LGS TT M1–M4) to stabilize the LGS image at the inside focus, 3) relay lenses (L1 & L2) to convert the focal ratio into  $f/65$ , 4) an ADC for the NGS beam, 5) a vibrating membrane mirror (VM) with a phase monitor, 6) collimating mirrors (M6–M8), 7) a lenslet array coupling to APDs through optical fibers, 8) an acquisition/mapping CCD camera (AQ CAM) with a 20 arcsec FOV, 9) a high-resolution camera (Hi-RES CAM) with a pixel scale of a few milli-arcsec, and 10) a pupil camera. The last two cameras are video-rate cameras used for alignment and diagnostic purposes.

Two operation modes are switched by changing the BS2 from a broad-band reflection mirror to a laser beam splitter for NGS and LGS. In the LGS mode, an additional tip-tilt correction of LGS is required. We will do this correction at the WFS rather than at the laser launching telescope. This correction should be done at the pupil to minimize the lateral shift of the pupil at the lenslet array. The Offner relay forms an additional pupil of 5.8 mm on the secondary mirror (M3) of the Offner relay, which is a convex spherical mirror mounted on a tip-tilt mount, and stabilizes the LGS image spot at the focus. The range of tilt of M3 is  $\pm 0.4$  degree, which corresponds to  $\pm 2$  arcsec on the sky. The imaging performance is insensitive to the tilt of M3, and no significant wavefront error is introduced by tilting of M3. In the NGS mode, this LGS TT optics is skipped by removing the M1 and M4 pickoff mirrors.

The FOV of this WFS is 4 arcsec in diameter, but the optics until the acquisition camera can transmit a 20 arcsec diameter field. The FOV of WFS is variable continuously with a motorized iris diaphragm located at front of the VM.

### 3.1.2. Lenslet Array

The geometry of the lenslet array (Figure 3) is almost identical with one of DM except for the outermost lenslets. The geometry is optimized by simulation to maximize the performance.<sup>5</sup> The optical design is similar to one of the current NGS36 system. It is a plastic lens molded from a copper mold, and the mold will be very precisely machined by diamond tool in Nalux Co. in Osaka. Each lenslet focuses the incident rays into an optical fiber placed at the back surface of the fused silica plate. An index-matching oil will be used between the glass surface and fiber input to avoid the reflection. The size of the sub-aperture is increased by about twice from one of the current system in order to make assembling easier by increasing a space between optical fibers. The surface figure of the lenslets is aspherical to form an enough small image spot to achieve a high coupling efficiency with the optical fiber even for the large innermost and outermost lenslets. Figure 4 shows the imaging performance of the lenslets.

We will use a custom aspherical molded lens instead of the standard gradient index lens of the APD module for the fiber-to-APD coupling in order to achieve a wider spectral coverage of 0.45–1.0  $\mu\text{m}$ . This coupling lens

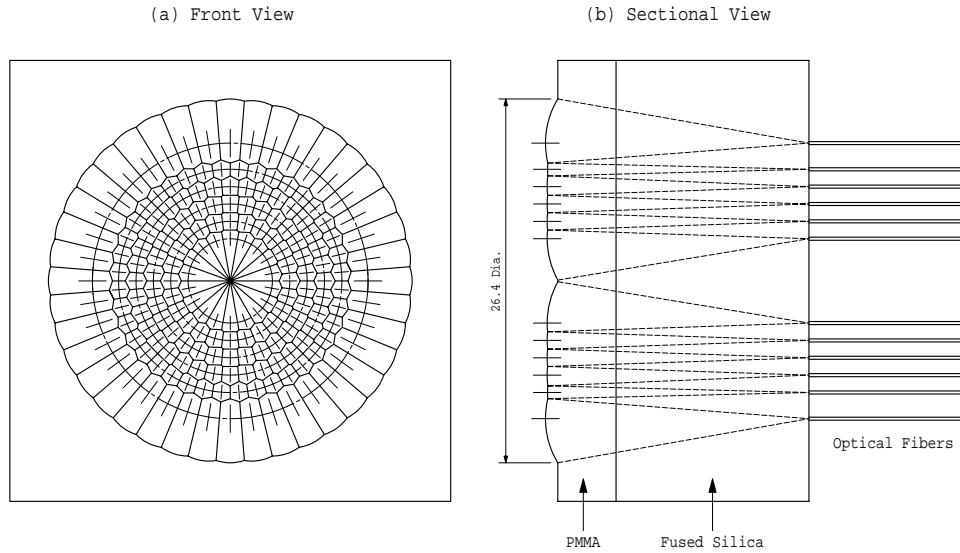


**Figure 3.** Design of high-order WFS lenslet array. The left (a) shows the geometry of the lenslet array, and the right (b) shows the sectional view. The dashed lines illustrate that each lenslet focuses the incident rays into an optical fiber placed at the back surface of the lenslet array. The diameter at the outer edge of the outer lenslet is 26.4 mm (the pupil diameter is 20 mm).

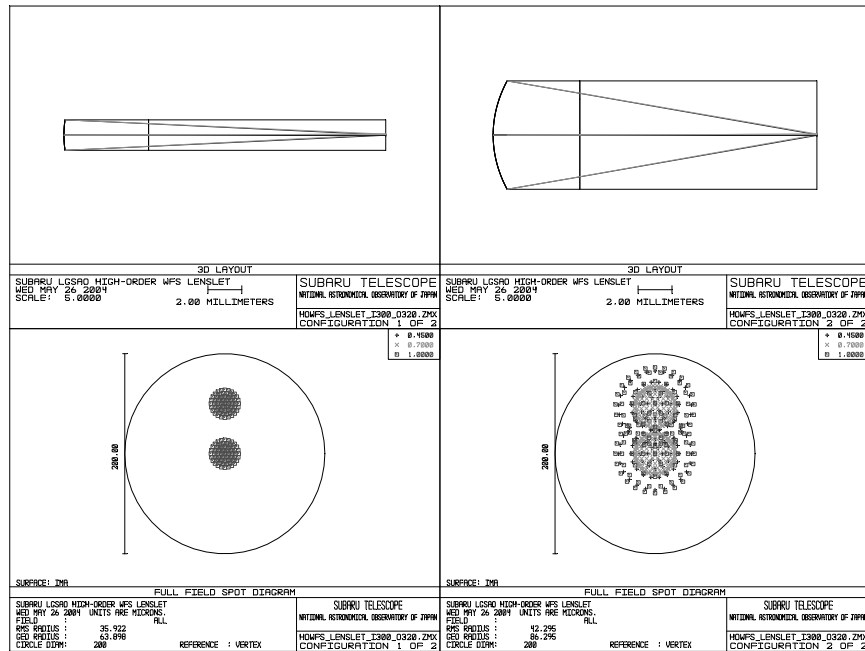


**Figure 4.** Lenslet imaging performance of high-order WFS lenslet array. The top and bottom boxes show the optical layout and spot diagram, respectively. The left and right show for the medium and innermost/outermost lenslets with a maximum aperture radius of 0.9 and 3.0 mm, respectively. Two spots corresponding to two field positions of 0 (on-axis) and 2 arcsec (edge of field of view) are presented for three wavelengths of 0.45, 0.7, and 1.0  $\mu\text{m}$ . The circles indicate the core size of a 200  $\mu\text{m}$  diameter of the optical fiber.

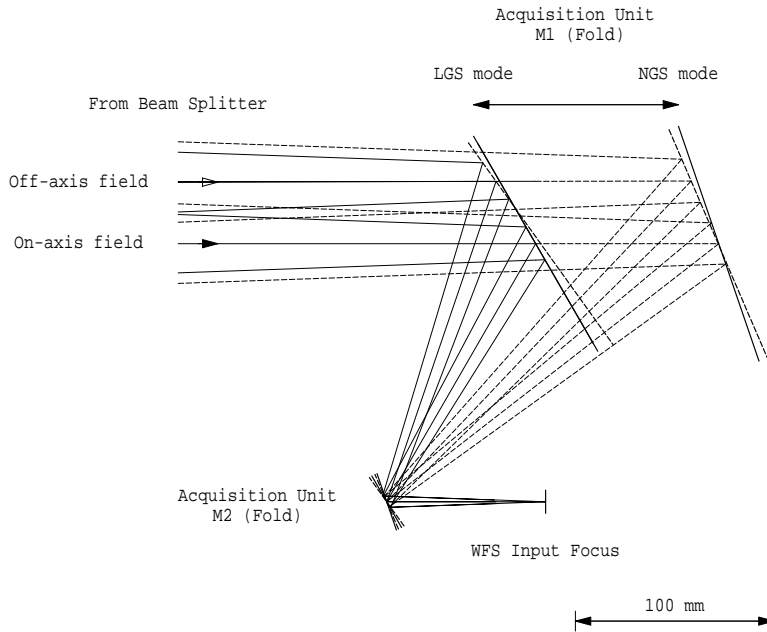


**Figure 5.** Optical layout of guide star acquisition unit aligned for on-axis (solid line) and off-axis (dashed line) field positions in the NGS and LGS modes.

relays the output beam from the optical fiber (core diameter =  $200\ \mu\text{m}$ ,  $\text{NA} = 0.26$ ) into the active area of  $175\ \mu\text{m}$  in diameter of the APD sensor. The current NGS36 system uses a similar aspherical lens for this purpose.

### 3.1.3. Guide Star Acquisition Unit

Unlike the current NGS36 system, as a guide star acquisition unit, we will adopt two steering fold mirrors mounted on two-axis gimbal mounts, similar to one of the Keck AO<sup>10</sup> and Gemini Altair system,<sup>11</sup> to reduce the loss of throughput by minimizing the number of mirrors. Figure 5 illustrates the acquisition unit aligned for on-axis and off-axis field positions in both NGS and LGS modes. The first mirror tilts to send a chief ray to the center of second mirror, and the second mirror tilts to align the chief ray with the input axis of WFS. The second mirror also slides along the input axis of WFS to keep the same travel distance for rays when the mirrors tilt for an off-axis field. It can compensate for a slight focal shift due to the field curvature produced by the science path OAP relay. Two units are used for the high- and low-order WFSs.

In the LGS mode, there is a large focal shift of 61-154 mm depending on a distance of 80–200 km between the telescope and the sodium layer. In addition, it varies as a function of the time during the telescope’s tracking, since the distance to the sodium layer varies according to the zenith angle and the temporal variation of height of the sodium layer. We will compensate for this focal shift by the acquisition unit. It requires very high accuracy (nearly 1 arcsec) for the tilt motions of the mirrors to maintain the image position during tracking of the LGS focus. We have built and are testing a prototype of this acquisition unit, to check the feasibility before finalizing the design.

### 3.1.4. Optical Throughput

Table 3 shows the throughput estimates for the high-order WFS path including the telescope and science path but excluding the APD module. For the throughput from the lenslet to APD (= Lenslet-to-fiber  $\times$  Fiber-to-APD in the table), the estimate is similar to a measured value of about 0.9 for the current NGS36 system. The catalog values of the photon detection efficiency of the APD module are also shown in the table for reference.

The current NGS36 system uses a dichroic multilayer (DML) coating for most of the WFS mirrors, but an aluminum coating is used for the vibrating mirror. We will use a DML coating for all the WFS mirrors including the vibrating mirror to improve the throughput.

**Table 3.** Throughput estimates for high-order WFS path.

Wavelength ( $\mu\text{m}$ )	0.45	0.589	0.70	1.00
Telescope (1 Al + 2 Ag mirrors)	0.784	0.847	0.829	0.903
IMR (3 Ag mirrors)	0.804	0.918	0.913	0.947
AO (5 Ag mirrors)	0.696	0.868	0.859	0.913
BS1 (1 BS reflection)	0.950	0.950	0.950	0.950
AU1 (2 DML mirrors)	0.980	0.980	0.980	0.980
Lenslet-to-fiber (1 plastic surface)	0.980	0.980	0.980	0.980
Fiber-to-APD (3 surfaces)	0.941	0.941	0.941	0.941
<b>NGS mode</b>				
BS2 (1 DML mirror)	0.990	0.990	0.990	0.990
WFS (5 DML mirrors + 4 glass surfaces)	0.914	0.914	0.914	0.914
<b>Overall without ADC</b>	<b>0.341</b>	<b>0.524</b>	<b>0.505</b>	<b>0.606</b>
ADC (4 glass surfaces)	0.961	0.961	0.961	0.961
<b>Overall with ADC</b>	<b>0.328</b>	<b>0.504</b>	<b>0.485</b>	<b>0.582</b>
<b>LGS mode</b>				
BS2 (1 BS reflection)		0.950		
WFS (10 DML mirrors + 4 glass surfaces)		0.869		
<b>Overall</b>		<b>0.479</b>		
APD photon detection efficiency	0.28	0.66	0.73	0.16

### 3.2. Visible Low-order WFS

The visible low-order WFS measures tip-tilt and slow defocus terms of wavefront by using a single visible NGS when LGS is used in the high-order WFS. The Shack-Hartmann (SH) sensor is chosen to optimize the wavefront tilt sensing performance also with defocus measurement capability. This is a  $2 \times 2$  sub-aperture SH sensor with 16 APD modules, and includes 1) a beam splitter (BS2) to split the light into the laser and natural light, 2) a guide star acquisition unit (AU2) to acquire a guide star from a 2.7 arcmin diameter field, 3) relay lenses (L1 & L2), 4) an ADC, 5) a collimating lens (L3), 6) a  $2 \times 2$  SH lenslet array, 7) a  $4 \times 4$  detector lenslet array coupling to APDs through optical fibers, and 8) a acquisition/mapping CCD camera (AQ CAM) with a 20 arcsec FOV.

The SH lenslet array divides the pupil with a 5 mm diameter into a  $2 \times 2$  array. The number of the detector lenslets per one SH sub-aperture is  $2 \times 2$ , and the total number of the detector lenslets is 16. The FOV of this WFS is 3.5 arcsec in diameter, and is variable continuously with a motorized iris diaphragm located at the intermediate focus.

### 3.3. Infrared Low-order WFS

We have a future upgrade option for measurement of tip-tilt and slow defocus terms of wavefront in the infrared region instead of the visible region, when no visible NGS is available around the science target for the visible low-order WFS. This will be a  $2 \times 2$  sub-aperture SH sensor with a  $128 \times 128$  pixel HgCdTe array from Rockwell.

## 4. CALIBRATION UNIT

The calibration unit is a source simulator for alignment, calibration, and diagnostics purposes. This unit is insertable in front of the IMR of the AO module. It simulates LGS and NGS beams, simultaneously, with and without turbulence by two turbulent layers of about 0 and 6 km altitudes, and reproduces the anisoplanatism and the cone effect for the LGS beam. It includes 1) laser and natural light sources, 2) two collimating lenses (L1 & L2) to collimate the input beam from the light sources, 3) a beam splitter to couple natural and laser light paths together, 4) two rotating turbulent plates (TP), and 5) re-imaging lenses (L3 & L4) to produce the  $f/13.9$  beam on the telescope focal plane.

We will use a turbulent plate similar to that in the current NGS36 system. This is a molded plastic plate with a deformed surface to produce a wavefront error with Kolmogorov statistics, and was made from the copper

mold machined by diamond tool in a similar manner to that of the lenslet array of the current system. The turbulent plate in the current system has a diameter of 30 mm, a thickness of 2 mm, and the beam diameter is about 9 mm. In the new system, the beam diameter becomes larger, 16 mm, and a larger diameter of about 100 mm is required, but the structure scale of the deformed surface will be expanded according to the beam diameter.

## 5. OPTICAL ERROR BUDGET

Our goal for the non-common path error is 40 nm rms in wavefront. The major contribution of the non-common path error is expected to be from the surface figure irregularity of the BS1 (about 20–40 nm rms in wavefront), because of difficulty in achieving a high accurate surface of CaF<sub>2</sub> relative to normal glasses. The common path error during AO closed-loop is expected to be mainly from the surface error of the DM (32 nm rms in wavefront).

## ACKNOWLEDGMENTS

This project is supported by a Grant-in-Aid for Scientific Research of the Ministry of Education, Culture, Sports, Science, and Technology.

## REFERENCES

1. Y. Hayano, H. Takami, W. Gaessler, N. Takato, M. Goto, Y. Kamata, Y. Minowa, N. Kobayashi, and M. Iye, "Upgrade plans for Subaru AO system," *Proc. SPIE* **4839**, pp. 32–43, 2003.
2. H. Takami, N. Takato, M. Otsubo, T. Kanzawa, Y. Kamata, K. Nakashima, and M. Iye, "Adaptive optics system for Cassegrain focus of Subaru 8.2 m telescope," *Proc. SPIE* **3353**, pp. 500–507, 1998.
3. H. Takami, N. Takato, Y. Hayano, M. Iye, S. Oya, Y. Kamata, T. Kanzawa, Y. Minowa, M. Otsubo, K. Nakashima, W. Gaessler, and D. Saint-Jacques, "Performance of Subaru Adaptive Optics System," *PASJ* **56**, pp. 225–234, 2004.
4. H. Takami, M. Iye, Y. Hayano, Y. Saito, Y. Kamata, N. Arimoto, N. Takato, S. Colley, M. Eldred, T. Kane, O. Guyon, S. Oya, M. Watanabe, M. Hattori, M. Goto, N. Kobayashi, and Y. Minowa, "Laser guide star AO project at the Subaru Telescope," *Proc. SPIE* **5490**, 2004.
5. O. Guyon, N. Arimoto, S. Colley, M. Eldred, M. Goto, M. Hattori, Y. Hayano, M. Iye, Y. Kamata, T. Kane, N. Kobayashi, M. Watanabe, Y. Minowa, S. Oya, Y. Saito, H. Takami, and N. Takato, "Subaru Telescope LGS AO: overview of expected performances," *Proc. SPIE* **5490**, 2004.
6. S. Oya, O. Guyon, M. Watanabe, Y. Hayano, H. Takami, M. Iye, S. Colley, M. Eldred, T. Kane, M. Hattori, Y. Saito, Y. Kamata, N. Kobayashi, Y. Minowa, M. Goto, N. Arimoto, and N. Takato, "Deformable mirror design of Subaru LGS AO system," *Proc. SPIE* **5490**, 2004.
7. Y. Hayano, M. Iye, Y. Saito, Y. Kamata, N. Arimoto, H. Takami, N. Takato, S. Colley, M. Eldred, T. Kane, O. Guyon, S. Oya, M. Watanabe, M. Hattori, M. Goto, N. Kobayashi, Y. Minowa, N. Saito, K. Akagawa, and S. Wada, "Design of laser system for Subaru LGS AO," *Proc. SPIE* **5490**, 2004.
8. R. Donaldson, D. Bonaccini, J. Brynnel, B. Buzzoni, L. Close, B. Delabre, C. Dupuy, J. Farinato, E. Fedrigo, N. Hubin, E. Marchetti, S. Ströbele, and S. Tordo, "MACAO and its application for the VLT Interferometer," *Proc. SPIE* **4007**, pp. 82–93, 2000.
9. H. Bonnet, S. Ströbele, F. Biancat-Marchet, J. Brynnel, R. Conzelmann, B. Delabre, R. Donaldson, J. Farinato, E. Fedrigo, N. Hubin, M. Kasper, and M. Kissler-Patig, "Implementation of MACAO for SINFONI at the Cassegrain focus of VLT, in NGS and LGS modes," *Proc. SPIE* **4389**, pp. 329–343, 2003.
10. D. S. Acton, P. L. Winzinowich, M. Divittorio, and T. Gregory, "Lessons learned in the design, construction, and implementation of the W. M Keck Observatory AO system," *Proc. SPIE* **4007**, pp. 14–25, 2000.
11. E. H. Richardson, J. M. Fletcher, C. L. Morbey, J. M. Oschmann, and J. S. Pazder, "Optical design of Gemini Altair," *Proc. SPIE* **3353**, pp. 600–610, 1998.